

# Effects of confinement and vaccination on an epidemic outburst: a statistical mechanics approach

Óscar Toledano,<sup>1</sup> Begoña Mula,<sup>2</sup> Silvia N. Santalla,<sup>3</sup> Javier Rodríguez-Laguna,<sup>2</sup> and Óscar Gálvez<sup>1</sup>

<sup>1</sup>*Dpto. Física Interdisciplinar, UNED, Madrid (Spain)*

<sup>2</sup>*Dpto. Física Fundamental, UNED, Madrid (Spain)*

<sup>3</sup>*Dpto. Física & Grupo Interdisciplinar de Sistemas Complejos,*

*Universidad Carlos III de Madrid, Leganés (Spain)*

(Dated: February 20, 2021)

This work describes a simple agent model for the spread of an epidemic outburst, with special emphasis on mobility and geographical considerations, which we characterize via statistical mechanics and numerical simulations. As the mobility is decreased, a percolation phase transition is found separating a free-propagation phase in which the outburst spreads without finding spatial barriers and a localized phase in which the outburst dies off. Interestingly, the number of infected agents is subject to maximal fluctuations at the transition point, building upon the unpredictability of the evolution of an epidemic outburst. Our model also lends itself to test with vaccination schedules. Indeed, it has been suggested that if a vaccine is available but scarce it is convenient to select carefully the vaccination program to maximize the chances of halting the outburst. We discuss and evaluate several schemes, with special interest on how the percolation transition point can be shifted, allowing for higher mobility without epidemiological impact.

## I. INTRODUCTION

Epidemic containment has been a crucial problem for humankind throughout our history, which has become of paramount importance since the COVID-19 outbreak late in 2019. The efforts to understand the spread of infectious diseases have attracted a large variety of professionals from all scientific fields, ranging from biology to sociology (see recent studies from different fields: [1–3]). Mathematical modeling has also provided very relevant tools to analyze the stream of data concerning the infected population, and has substantially contributed to policy design (see e.g. [5, 6, 15]). Among different approximations employed, agent-based models have been extensively used to provide policy recommendations even in the COVID-19 case [7], for which simulations based on stratified population dynamics were recently carried out [8]. Multiscale approaches are known to improve our ability to explain the geographical expansion of the disease, and they have been also used, along data-driven simulations, to analyze the epidemic of COVID-19 in Brazil [9]. Epidemic waves have also been considered [9, 10] employing stratified population dynamics and non-autonomous dynamics, where mitigation effects are subsequently imposed and relaxed.

During the COVID-19 epidemic, and due to the scarce amount of vaccination doses in the first instants of the vaccination campaign, immunization schedules have also attracted attention of the modeling community with the aim of stifling the expansion of an epidemic burst by removing a number of nodes substantially below the percolation threshold [11] through the search of certain types of motifs in the contact network.

However, predictions about the evolution of an epidemic burst are known to be difficult and unreliable, because the uncertainty in the initial data propagates

exponentially [12]. Yet, on occasions the inherently unpredictability of the models can be turned in our favor. Here we claim that the fluctuations in the number of infected people during the evolution of an epidemic burst can provide useful information regarding our ability to stifle an ongoing epidemic.

In this work, we propose a very simple agent model [13] of the susceptible-infected-recovered (SIR) type [14],[15]. Agents follow a random walk in the vicinity of their homes, which are randomly distributed on a square lattice, wandering up to a maximum distance  $R$ , which may vary from agent to agent. When  $R$  is very short, agents are effectively confined at home, and an infectious outbreak will very likely die off. As this distance is increased, outbreaks have larger chances of spreading throughout the system, until a percolation phase transition is reached, [16] in which the presence of an infinite cluster becomes certain. Further increases of mobility will have a very limited impact on the spread of the infectious disease. Interestingly, predictions about the future evolution of the epidemic are more difficult at the transition point. Indeed, above the percolation threshold the mean-field theory associated with the SIR equations provide a very accurate prediction of the evolution of the model, while below the transition point typical outbursts will not propagate beyond a certain correlation length. But when the agent mobility approaches to the percolation value, the precise geographical origin of the outbreak becomes crucial to predict the outcome. Even though an infinite connected cluster exists, the probability that the initial infected agent will be part of it is minimal at that point, leading to maximal uncertainty. Thus, we show that the fluctuations in the number of infected people become a very useful observable in order to pinpoint the phase transition.

Of course, our model is far too simple to be taken decisively in order to provide policy recommendations, which

should be always undertaken with the assessment of experts from several fields. Yet, our results suggest that lock-down measures are either useless, when the system remains much above the percolation threshold, or effective, once it has been crossed. Finding that phase transition is therefore of paramount importance, and a very difficult task. We can not provide a complete recipe to establish that threshold in practice, but we provide an interesting proxy: fluctuations in the infection reach.

If an effective vaccine is available but scarce, a vaccination schedule becomes unavoidable, i.e.: the determination of the agents which must be immunized in order to minimize the spread of the infection. Of course, many individuals should receive the vaccine because of other considerations, such as age, health condition or profession and we will not discuss these very relevant aspects. Our model lends itself very easily to the evaluation of the efficiency of a vaccination program. In it, individuals are only distinguished through their relations: some homes are relatively isolated, so their inhabitants are not likely to spread the disease. Yet, a naive approach would consider that individuals with many connections should be the first candidates to be immunized. We will prove that this criterion is not optimal. Indeed, some agents with few connections act as natural *bridges* between different clusters. Thus, if they receive the vaccine the clusters will become isolated and the outburst will be halted.

This article is organized as follows. Sec. II discusses in detail our agent model, and how our numerical simulations are performed. In Sec. III and IV we describe our results regarding the percolation phase transition as the agent mobility or recuperation probability are increased. The efficiency of several vaccination schemes is discussed in Sec. V, specially in connection with the shift of the percolation threshold. Our conclusions and ideas for future work are discussed in Sec. VI.

## II. THE CONFINED-SIR MODEL

We propose a very simple model to characterize the effects of partial confinement in epidemic expansion, which we call the *confined-SIR* model.

### A. Description of the model

Let us consider  $N$  agents moving on an  $L \times L$  square lattice with periodic boundary conditions. Agent  $i$  possesses a *home*, determined by a fixed lattice point,  $\vec{H}_i$ . Agents can move freely within their *wandering circles*, centered at  $\vec{H}_i$  and with radius  $R_i$ . Time advances in discrete steps  $\Delta t = 1$ , in arbitrary units. At each time, each agent takes a random step within their wandering circles with equal probability, and if the step leads to a forbidden position, a new step is attempted. We will assume that homes are distributed randomly over the whole lattice.

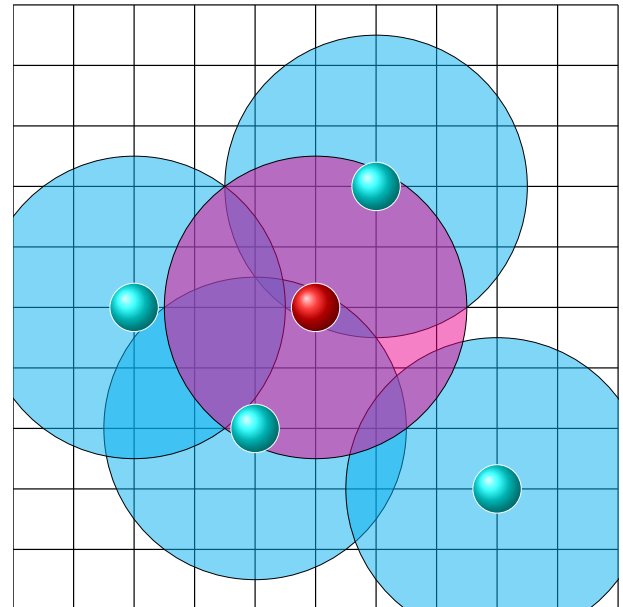


Figure 1. Illustration of the confined SIR model. The red agent at the center is infected, and can move freely within its wandering circle, shown in magenta. The blue agents are susceptible, and can move within their wandering circles, shown in cyan. Notice that the magenta circle intersects all cyan circles, thus providing a finite probability of infection for all those agents.

Agents can be classified into three groups: susceptible ( $S$ ), infected ( $I$ ) and recovered ( $R$ ). Susceptible agents get infected with probability  $\beta$  when they share cell with an infected agent. Infected agents may get recovered at each time-step, with probability  $\gamma$ . An illustration can be seen in Fig. 1.

Our aim is to determine the probability distribution for the number of infected agents, with special interest in the asymptotic values, i.e. the total number of agents that have suffered the infection in the long run. In some cases, an effective SIR model can be written down and solved analytically.

The dynamics of the model can be approximated by a Markov chain. Let us consider that, at time  $t$ , we know the epidemiological status of each agent,  $s_i \in \{S, I, R\}$ , the location of their home  $H_i$  and their wandering radii,  $R_i$ . From these data we can estimate the transition probabilities for each agent.

Let  $A_i$  stand for the number of lattice points in the wandering circle of agent  $i$ , while  $A_{ij}$  will stand for the number of lattice points in the intersection between the wandering circles of agents  $i$  and  $j$ . The probability that agent  $i$  and agent  $j$  will collide at time  $t$  can be estimated as

$$C_{ij} = \frac{A_{ij}}{A_i A_j}. \quad (1)$$

Thus, if agent  $s_i = I$  and  $s_j = S$ , the probability per unit time that agent  $j$  will get infected becomes  $P_{ij}^I = \beta C_{ij}$ . Thus, we can find the probability per unit time that an agent  $i \in S$  will get infected just summing over all possible infection sources

$$P_i^I = \beta \sum_{j \in I} C_{ij} = \beta \sum_{j \in I} \frac{A_{ij}}{A_i A_j}. \quad (2)$$

The evolution of the expected number of infected agents can now be found,

$$\langle I(t+1) \rangle = (1 - \gamma) \langle I(t) \rangle + \beta \left\langle \sum_{\substack{i \in S \\ j \in I}} C_{ij} \right\rangle, \quad (3)$$

Notice that the  $C_{ij}$  do not change, but the right hand side changes due to the evolution in the identity of the agents in sets  $I$  and  $S$ .

In the homogeneous limit,  $R_i \sim L$  and all agents wander around the whole region. Therefore, all  $C_{ij} \sim 1/L^2$ . Thus, in a mean-field approximation Eq. (3) becomes

$$\langle I(t+1) \rangle \approx (1 - \gamma) \langle I(t) \rangle + \frac{\beta}{L^2} \langle S(t) \rangle \langle I(t) \rangle, \quad (4)$$

and we obtain the usual SIR differential equations. Introducing fractional variables,  $s = \langle S \rangle/N$ ,  $i = \langle I \rangle/N$  and  $r = \langle R \rangle/N$  we reach:

$$s(t+1) \approx s(t)(1 - \beta \rho i(t)) \quad (5)$$

$$i(t+1) \approx (1 - \gamma)i(t) + \beta \rho s(t)i(t) \quad (6)$$

$$r(t+1) \approx r(t) + \gamma i(t), \quad (7)$$

where  $\rho$  is the population density defined as:

$$\rho = N/L^2. \quad (8)$$

For early times,  $s(t) \approx 1$  so the infection either expands or vanishes depending on the value of the basic reproductive number, which in this case can be defined as

$$R_0 = \frac{\beta \rho}{\gamma}. \quad (9)$$

We will always assume  $R_0 > 1$ , i.e.: the infection will propagate in the total mixing approximation.

## B. Effective network

Within the confined-SIR model, the infection can propagate between agents  $i$  and  $j$  only if  $C_{ij} > 0$ . This condition determines an effective network,  $\mathcal{G}$ , such as the ones shown in Fig. 2, in which the homes are represented as

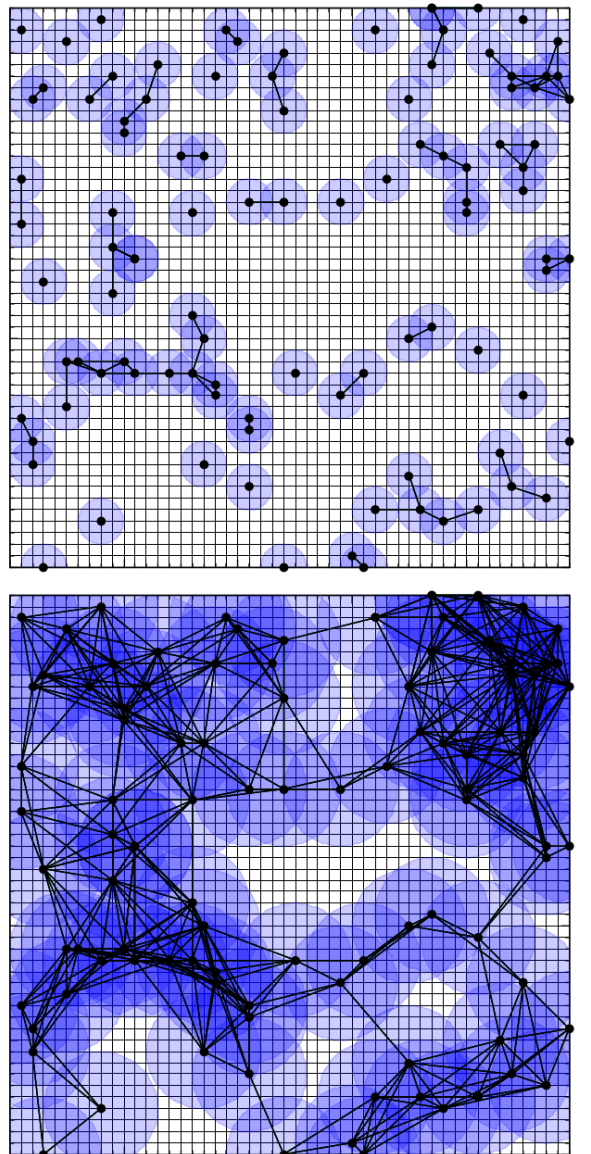


Figure 2. Effective networks obtained from a confined-SIR system using  $N = 100$  homes on a  $50 \times 50$  lattice. Nodes are associated with the homes of the agents, while links are drawn if their respective dwellers are able to meet during their wandering. Top: using  $R = 2$ ; bottom: using  $R = 5$ .

nodes of a graph, and the links denote the pairs of agents that are able to meet. Both networks are obtained for  $N = 100$  agents on  $50 \times 50$  lattices, using  $R = 2$  (top) and  $R = 5$  (bottom). It can be readily seen that the network for  $R = 2$  contains many disconnected clusters, while for  $R = 5$  it contains a large cluster spanning most of the nodes.

### C. Numerical simulations

We have run numerical simulations of our confined-SIR model on a square lattice, placing  $N$  random homes and using the same value of the wandering radius  $R$  for all agents. Unless otherwise specified, we always average over  $N_S = 5000$  samples, with fixed values for  $\beta = 1$  and  $\gamma = 0$ ,  $N = 1000$  agents and  $\rho = 5 \cdot 10^{-6}$ . Thus, the average distance between homes,  $\bar{r}$  (eq. 10), and the size of the lattice are determined by density values and the number of agents considered.

In the case of large values of the wandering radius  $R$ , we expect the behavior to correspond to the mean-field approximation provided by the SIR equations for perfect mixing. We have checked that conjecture numerically, and the results are shown in Fig. 3 (top panel). The correspondence between our parameters and the parameters of the SIR model is immediate. However, for low values of the mobility parameter  $\varepsilon$ , we see in bottom panel of Fig. 3 that the average curve significantly deviates from the solutions of the SIR equations because the assumptions of perfect mixing do not hold.

### III. PERCOLATION PHASE TRANSITION

The theory of bond percolation has been one of the foremost paradigms of statistical mechanics for more than forty years [17–20], with applications to magnetism [21], wireless communications [22], ecological competition [23] or sequence alignment in molecular biology [24]. Recently, a very relevant connection was described between the geodesics in strongly disordered networks and bond percolation [29]. Application of percolation theory to epidemics has been carried out by previous authors, such as [25, 26] or more recently [27, 28].

Bond percolation on a fixed lattice is characterized by a single parameter,  $p$ , the probability that a given bond will be present. Above a certain threshold value,  $p > p_c$ , the probability that the system will contain an infinite connected cluster reaches one, with  $p_c = 1/2$  for the square lattice. Our system presents a strong similarity with bond percolation, but with another observable playing the role of the bond probability  $p$ . Let us consider  $N$  agents on an  $L \times L$  lattice. The average distance between homes,  $\bar{r}$ , can be estimated as

$$\bar{r} = \frac{L}{\sqrt{N}}. \quad (10)$$

Now, let us notice that the wandering radius  $R$  is only meaningful when compared to this average distance between homes. Thus, we introduce a *mobility parameter*,

$$\varepsilon = \frac{R}{\bar{r}} = \frac{R\sqrt{N}}{L}. \quad (11)$$

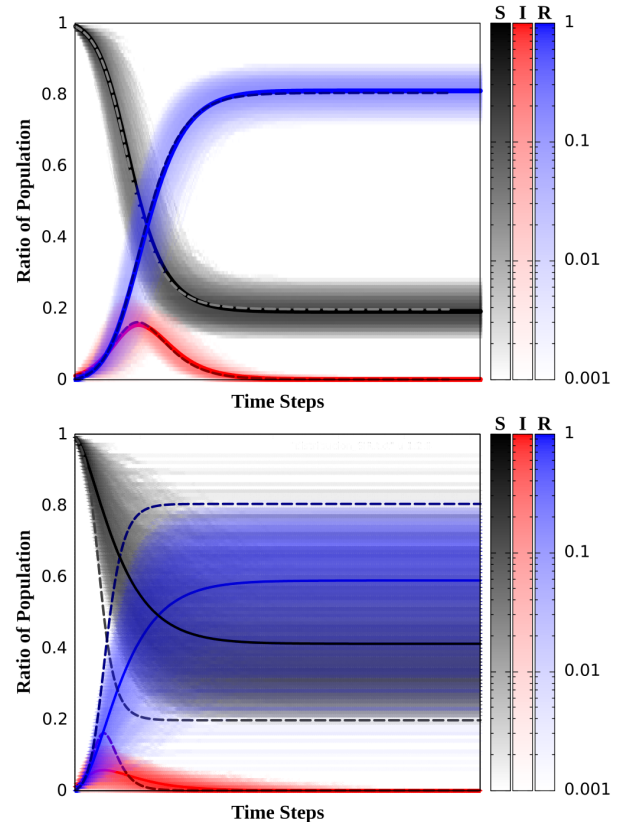


Figure 3. Top: Average number of susceptible, infected and recovered agents as a function of time, depicted with continuous black, red and blue lines respectively, as obtained using  $\beta = 0.02$ ,  $\gamma = 5 \cdot 10^{-4}$ ,  $L = 141$ ,  $N = 1000$  and  $\varepsilon = 9.0$  (see eq. 11), and compared to the solution of the deterministic SIR equations, represented with dashed lines, being 1% the ratio of initial infected agents. Bottom: results from analogous simulations, with the mobility parameter value  $\varepsilon = 2.0$ , are represented. Probability distributions of the values obtained in the simulations are also represented with the logarithmic color scale.

We will readily show that the mobility parameter  $\varepsilon$  is the only relevant variable to determine the geometry of our system.

Critical points, such as the percolation transition, typically lead to large fluctuations. Thus, we have considered a new observable: the standard deviation of the fraction of infected agents,  $\sigma_I$ , which is shown in Fig. 4 (top panel) as a function of the mobility parameter, for different lattice sizes and densities. Indeed, we can observe that the fluctuations in the number of infected agents present a maximum for a certain value of  $\varepsilon$  which only depends on the ratio between the recovery and infection probabilities,  $\beta/\gamma$ .

Let us provide evidence that this critical value of the mobility parameter,  $\varepsilon_c$ , corresponds to the position of the percolation phase transition. In the vicinity of the percolation phase-transition many observables show critical behavior in the form of power laws. The most salient of

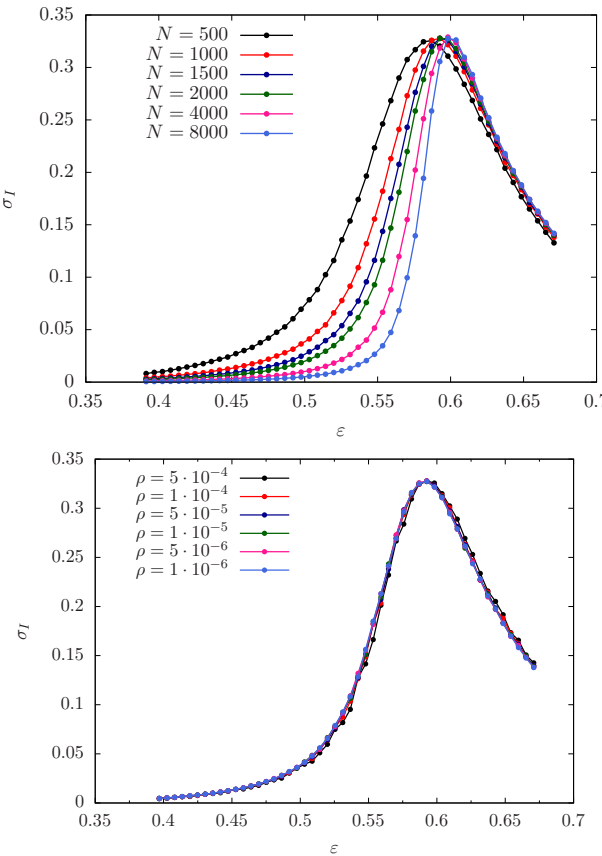


Figure 4. Top: Standard deviation of the fraction of infected agents as a function of the mobility parameter  $\varepsilon$ , for different numbers of agents and a fixed density  $\rho = N/L^2 = 5 \cdot 10^{-6}$ . Bottom: Standard deviation of the number of infected agents as a function of the mobility parameter using  $N = 1000$  agents for several values of the agent density  $\rho$ . Notice the collapse of all curves, using  $\beta = 1$  and  $\gamma = 0$ .

those is given by the average size of a cluster,  $s$ . Below the transition, we have

$$\langle s \rangle \sim |p - p_c|^{-\eta}, \quad (12)$$

with  $\eta = 43/18 \approx 2.39$  for a square lattice [16]. Fig. 5 shows the average cluster size of our effective networks as a function of the mobility parameter  $\varepsilon$ , for different system sizes and populations. We can observe that, for all system sizes considered, the average size of the cluster diverges as we approach a critical value  $\varepsilon_c$ , with an exponent which slightly differs from the value obtained in the square lattice,  $\eta \approx 2.35$ . This new value for the critical exponent  $\eta$  seems to be robust under changes in the lattice size and the density.

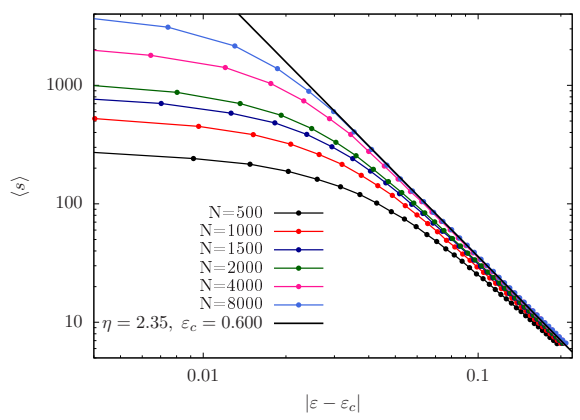


Figure 5. Average cluster size as a function of  $\varepsilon - \varepsilon_c$ , using  $\rho = 5 \cdot 10^{-6}$ ,  $\beta = 1$  and  $\gamma = 0$ . Notice the power-law behavior, following Eq. (12), with an exponent  $\eta \approx 2.35$ .

#### IV. NON-ZERO RECUPERATION PROBABILITY

It is relevant to discuss how does the situation change when there is a non-zero recuperation probability,  $\gamma > 0$ . In that case, infected agents may recover before they can propagate the disease, and thus we are led to compare two natural times:  $\tau_{ij} \approx C_{ij}^{-1}$  is the expected time before the infection may propagate from agent  $i$  to agent  $j$  (or viceversa), while  $\tau_R \approx \gamma^{-1}$  corresponds to the expected time before recovery. Thus, if  $\tau_{ij} \gg \tau_R$  we may assume that the infection will not be able to propagate from agent  $i$  to agent  $j$ , while in the opposite case,  $\tau_R \gg \tau_{ij}$  we may neglect the possibility of recovery. We may claim that a finite recuperation probability provides an effective cutoff for the local infection probabilities, thus removing weak links from the graph.

Fig. 6 (top panel) shows the standard deviation or fluctuations in the number of infected nodes as a function of the mobility parameter as we increase the recovery probability per unit time,  $\gamma$ . We notice that the fluctuation level at the maximum does not depend strongly on  $\gamma$ . In addition, the value of mobility parameter at which this maximum takes place grows quickly with  $\gamma$ . Thus, we are led to claim that the recovery probability per unit time affects the value of the percolation threshold. Also we can see in Fig. 6 that for low  $\gamma$  values the fluctuations peak in a maximum as it was shown in Fig. 4, while it is reach a plateau for higher values of  $\gamma$ . When the number of final infected agent along increasing  $\gamma$  values is calculated (bottom panel of Fig. 6), we observed a continuous decrease of  $\langle s \rangle$  for higher recuperation probability, as expected.

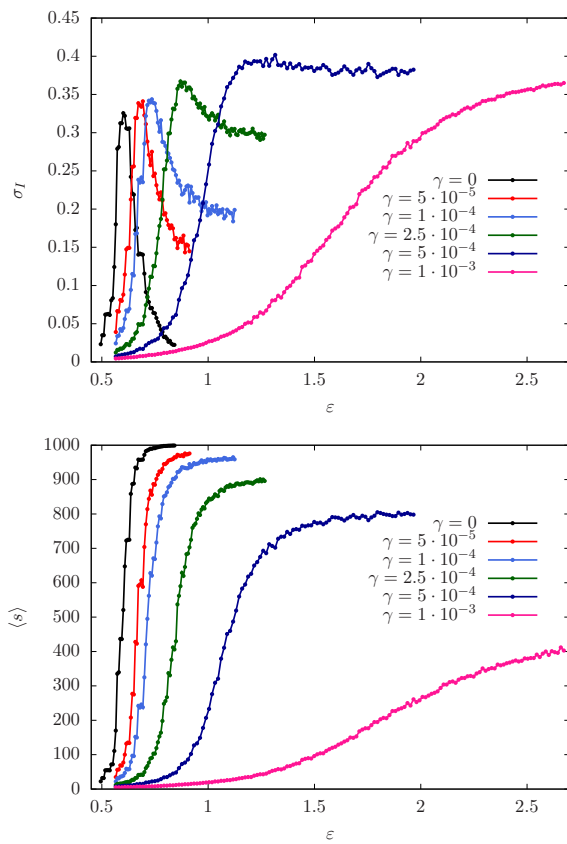


Figure 6. Top: Standard deviation of the number of infected nodes as function of the mobility parameter for different values of the  $\gamma$  parameter. Bottom: number of final infected agents as function of the mobility parameter for different values of the  $\gamma$  parameter. Simulations were performed with  $N = 1000$ ,  $N_S = 5000$  samples,  $\beta = 1$  and  $\rho = 5 \cdot 10^{-3}$ .

## V. VACCINATION SCHEDULES

Let us consider the possibility of providing immunity through vaccination to a certain (small) fraction of the population,  $f_v$ . In this section we will attempt to answer the following questions: how to select the agents that will receive the vaccine, if our only aim is to minimize the spread of a future epidemic outburst. Notice that, in practice, many other issues must be considered in this situation, such as the health conditions or the age of the patients.

The simplest vaccination schedule is merely to select randomly the individuals. Of course, we do not expect this schedule to be very efficient. We have considered several observables which can be employed to determine how useful it will be to provide the vaccine to a certain agent. The simplest one is the *total degree*, defined as the number of first neighbors in the effective graph. Naively, we might sort the agents by their degrees, and immunize the first  $f_v N$ . Yet, it is more efficient to *recompute* the degree of each agent after each selection, and we will do so unless otherwise specified.

We can also define a *fragmentation degree* associated to an agent, intuitively defined as the relative increment of the local distance when he/she is removed. For any agent  $i$ , we can define its local distance  $S_i(A_i)$  as sum of all the distances between the agents  $A_i = \{j | C_{ij} > 0, j \neq i\}$ , i.e. the neighbors of  $i$ . Fragmentation of agent  $i$  is thus defined as

$$F_i = 1 - \frac{S(A_i \cup i)}{S(A_i)} \quad (13)$$

The most promising observable is, nonetheless, the *betweenness-centrality* [30] associated to each agent,  $BC_i$ , defined as the fraction of the total number of geodesics which go through agent  $i$ . This measure, indeed, is global, and takes  $O(N^4)$  steps to compute using Dijkstra's algorithm to evaluate the geodesics, while we are considering the case where the  $BC_i$  is recalculated after each vaccination [31]. In previous studies vaccination schemes based on immunizing the highest-betweenness links have proved to be very efficient (see e.g. [32]). Thus, we have considered the following five vaccination schedules.

0. No vaccination, considered the base case.
1. Select randomly.
2. Select the agents with highest *degree* (HD).
3. Select the agents with highest *fragmentation* (HF).
4. Select the agents with highest *betweenness-centrality* (BC).

The vaccination programs effectively change the topological properties of the network whenever the removed agents are not selected at random. Thus, in Fig. 7 we can observe an specific example of a network where different vaccination schemes have been performed over the same amount of agents. In order to get insight, let us observe the cluster structure. For random vaccination, Fig. 7 (A), the large clusters remain untouched. For a degree-based vaccination scheme, Fig. 7 (B), we can see that links have been removed from the *core* of the clusters, but the clusters themselves remain connected. Indeed, immunizing the individuals with a large number of connections seems to have a low impact on the network structure in our case. The reason is that high-degree agents tend to be neighbors of other high-degree agents. Panel (C) of Fig. 7, on the other hand, shows that removing agents with a large fragmentation fraction can lead to much smaller clusters, but still some very large clusters remain active, leading to a likely propagation of an epidemic outburst to a large fraction of the population. Fig. 7 (D) shows the resulting network when the agents with a largest betweenness-centrality have been removed (with recalculation), and we can readily see that all large clusters have indeed disappeared.

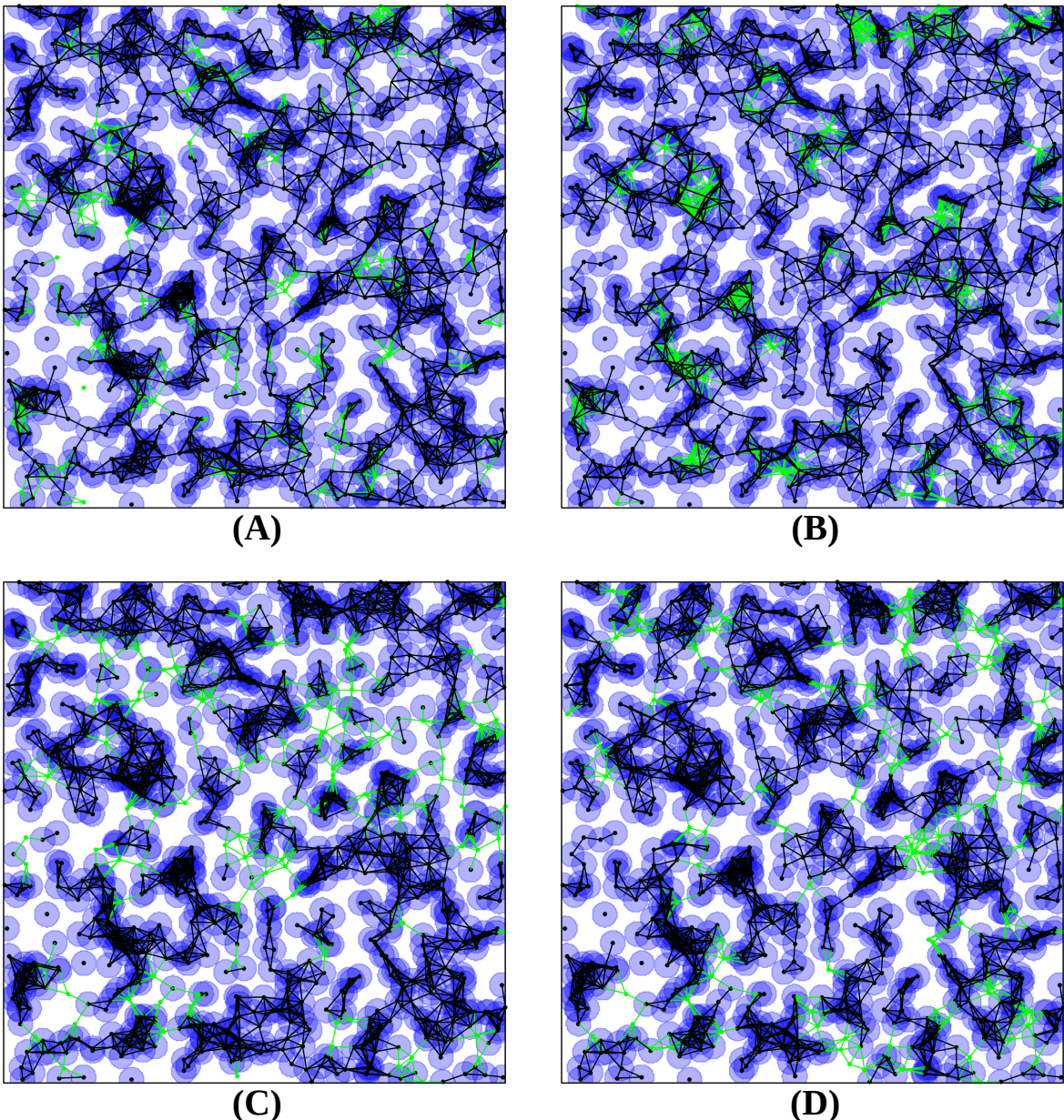


Figure 7. Effect of different vaccination schedules on a fixed network: (A) Random vaccination, (B) Highest degree, (C) Highest fragmentation, (D) Highest betweenness-centrality. Black dots denote susceptible agents, and they are joined by black links. Immunized agents are colored green, and the dead links are green. The parameters for all cases are  $N = 1000$ ,  $\varepsilon = 0.89$  and a 15% vaccination rate. Videos of numerical simulations for these vaccination schemes can be seen in <https://sites.google.com/view/epidemic-modelling-uned/home> [33]

In order to describe the quantitative effect of the different vaccination schedules, the top panel of Fig. 8 depicts the expected value of the total maximal number of infected agents as a function of the mobility parameter. The no vaccination case, marked with the black curve, reaches the total number of agents,  $N = 1000$ , with the transition at around  $\varepsilon_c \approx 0.6$ . The effect of the random vaccination scheme is analogous to that obtained by performing a reduction of the population density with a

factor  $1 - f_v$ , and thus the mobility parameter at the transition point will follow the relation  $\varepsilon_c = \varepsilon_c^0(1 - f_v)^{-1/2}$ , where  $\varepsilon_c^0$  stands for the critical value of the mobility parameter when no agents are vaccinated. Interestingly, random vaccination and highest degree vaccination provide similar outcomes, with a slightly higher critical value of the mobility parameter for the random case. Indeed, this shows that highest degree vaccination is not effective at all. Highest fragmentation vaccination, on the other

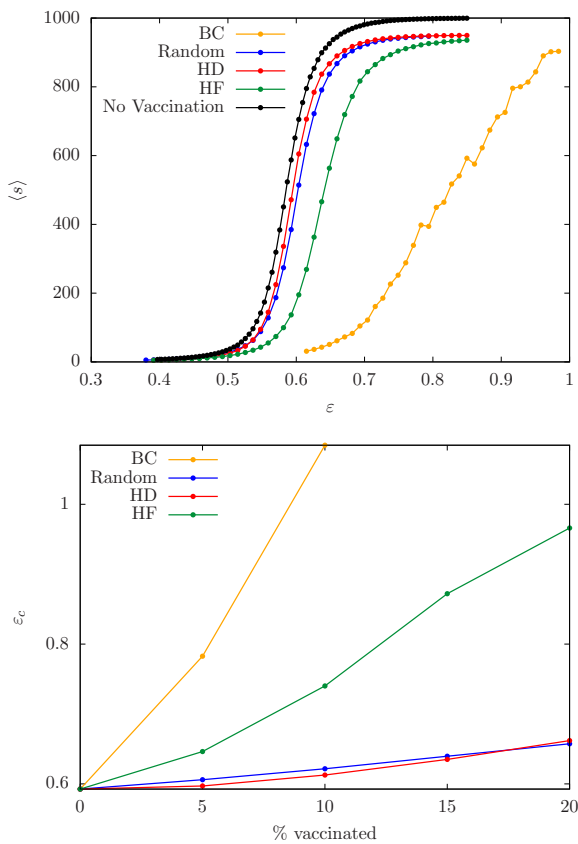


Figure 8. Top: Number of final infected agents for each vaccination schedule as a function of the mobility parameter  $\varepsilon$  with 5% of vaccinated agents. Bottom: Mobility parameter marking the percolation phase transition,  $\varepsilon_c$ , for each vaccination schedule along on the fraction of vaccinated agents considered.

hand, results in a substantial shift of the critical mobility parameter, being necessary to vaccinate only about 1/3 of the agents that in the case of random vaccination to obtain the percolation transition at the same mobility parameter value. Yet, the most effective vaccination schedule is, with a large difference, the one based on the highest betweenness-centrality (yellow line). In this case, we only need to vaccinate about 1/10 to obtain the same  $\varepsilon_c$  than in the case of random vaccination. This result is in agreement with previous studies [32]. Indeed, all schemes seem to reach a similar value of the total number of infected agents for large enough mobility parameters. Thus, we conclude that an effective vaccination scheme will increase substantially the mobility threshold under which an epidemic outburst will die off. Yet, the effects of vaccination can be substantially reduced above that mobility threshold.

How effective are the vaccination schedules shifting the percolation transition point? In order to answer that question we have traced the percolation threshold as a function of the ratio of immunized agents in the bottom panel of Fig. 8. The base value, for no vaccination, is

$\varepsilon_c \approx 0.6$  (as it is shown in Fig. 5). Betweenness-centrality vaccination results in a sharp displacement of the percolation transition, reaching  $\varepsilon_c \approx 1.1$  for  $\approx 10\%$  vaccination rate. Highest-fragmentation vaccination performs worse (0.74 for  $\approx 10\%$  vaccination), but still provides a significant improvement of the epidemiological situation for scarce vaccines. Random and high degree vaccinations perform similarly (0.62 for  $\approx 10\%$  vaccination), and none of them are quite effective.

## VI. CONCLUSIONS AND FURTHER WORK

In this work we have presented a very simple agent model for epidemic expansion in which the effects of partial confinements and vaccinations can be tested, and we have characterized its properties using tools from statistical mechanics, specially from percolation theory. Please notice that our model is far too simple to lead to policy recommendations without further insight from experts from different fields, ranging from virology to sociology. The main shortcoming of our model when applied to human epidemics is that human mobility is not geographically restricted in the same way as in our model. Indeed, even under lock-down essential workers must attend their workplaces, which might be very far away from their homes. Yet, we expect that some of our conclusions can be interesting for researchers in epidemic expansion and lead, in combination with insights from other specialists, to sensible policy recommendations which will help alleviate the effects of present and future epidemic outbursts.

Our first conclusion, in the confined-SIR model, is that confinement is basically useless much above the percolation threshold, and basically effective reasonably below it. Thus, it is of paramount importance to design lock-down measures so that mobility is restricted sufficiently below the percolation threshold, but it is useless to reduce mobility much below that point. The determination of the percolation threshold is not easy in practice, but a good hint is provided by the fluctuations in the sizes of the outbursts. Above the transition point, most outbursts reach a huge fraction of the population, and below it, it will only reach a few individuals. Yet, near the transition, the number of infected agents may vary enormously, depending on the location of the initial infected agent. In addition, the effect of increasing the recovery probability in our model causes a decrease of the number of final infected agents since it provides a efficient cut-off for the infection probability between pairs of agents which present low overlapping in their wandering areas.

Our second conclusion is that in order to determine an efficient vaccination schedule, disregarding other health-care considerations, *bridge* individuals should be targeted for vaccination, i.e. individuals which move between different clusters. Their immunization will lead to an effective confinement of an epidemic outburst to its initial cluster, thus creating effective firewalls be-

tween them. Bridge individuals can be detected via *betweenness-centrality*, which is a global and computationally expensive measure, or through easier proxies, such as the individual *fragmentation*. Fragmentation answers the question: *are your friends friends among them?* Individuals whose friends form a clique are not good candidates for vaccination, but individuals whose friends do not know each other are.

Confined SIR models seem an appropriate tool in order to improve our intuition regarding the effectiveness of different strategies to stifle an epidemic outburst and to find relevant observables in order to provide relevant observables which characterize the current situation and allow us to make meaningful predictions. For example, in this work we have emphasized the very interesting role provided by the fluctuations in the maximal number of

infected agents. Indeed, a very promising line of research is the statistical analysis of these fluctuations during real epidemic outbursts, such as COVID-19. These analysis present a very interesting challenge: fluctuations should be compared *ceteris paribus*, i.e. removing major differences between the different geographical areas and times.

## ACKNOWLEDGMENTS

We would like to acknowledge J.E. Alvarellos, P. Córdoba-Torres, R. Cuerno, E. Korutcheva and S. Ferreira for very useful discussions. This work was funded by Instituto de Salud Carlos III (Spain) through grant COV20/01081, and the Spanish government through grants PGC2018-094763-B-I00, PID2019-105182GB-I00 and PID2019-107514GB-100.

---

[1] B. Hu, H. Guo, P. Zhou and Zheng-Li Shi, *Characteristics of SARS-CoV-2 and COVID-19*, Nat. Rev. Microbiol. **19**, 141, (2020).

[2] L. Wynants et al, *Prediction models for diagnosis and prognosis of covid-19: systematic review and critical appraisal*, BMJ, **369**:m1328 (2020).

[3] L.J. Thomas, P. Huang, F. Yin, X.I. Luo, Z.W. Almquist, J.R. Hipp and C.T. Butts, *Spatial heterogeneity can lead to substantial local variations in COVID-19 timing and severity*, PNAS, **117**, 39, (2020).

[4] X. Li, J. Guo, C. Gao, L. Zhang and Z. Zhang, *A hybrid strategy for network immunization*, Chaos, Solitons & Fractals, **106**, 214–219, (2018).

[5] L. Hébert-Dufresne, A. Allard, J-G. Young and L.J. Dube, *Global efficiency of local immunization on complex networks*, Sci. Rep., **3**, 2171 (2013).

[6] S. Riley, K. Eames, V. Isham, D. Mollison, P. Trapman, *Five challenges for spatial epidemic models*, Epidemics **10**, 68–71, (2015).

[7] A. Aleta et al. *Modelling the impact of testing, contact tracing and household quarantine on second waves of COVID-19*, Nature Human Behaviour **4**, 964 (2020).

[8] A. Arenas, W. Cota, J. Gómez-Gardeñes, S. Gómez, C. Granell, J.T. Matamalas, D. Soriano-Paños, B. Steinegger, *Modeling the Spatiotemporal Epidemic Spreading of COVID-19 and the Impact of Mobility and Social Distancing Interventions*, Phys. Rev. X **10**, 041055 (2020).

[9] G.S. Costa, W. Cota, S.C. Ferreira, *Outbreak diversity in epidemic waves propagating through distinct geographical scales*, Phys. Rev. Research **2**, 043306 (2020).

[10] G.A. Muñoz-Fernández, J.M. Seoane, J.B. Seoane-Sepúlveda, *A SIR-type model describing the successive waves of COVID-19*, Chaos, Solitons and Fractals **144**, 110682 (2021).

[11] G.S. Costa, S.C. Ferreira, *Nonmassive immunization to contain spreading on complex networks*, Phys. Rev. E **101**, 022311 (2020).

[12] M. Castro, S. Ares, J.A. Cuesta, S. Manrubia, *The turning point and end of an expanding epidemic cannot be precisely forecast*, PNAS **117**, 26190 (2020).

[13] O. Toledano, B. Mula, S.N. Santalla, O. Gálvez and J. Rodríguez-Laguna, *Confined SIR model for epidemic expansion*, software repository, [https://github.com/jvrlag/confined\\_sir](https://github.com/jvrlag/confined_sir) (2021).

[14] W. O. Kermack, A. G. McKendrick, *A contribution to the mathematical theory of epidemics*. Proc. R. Soc. Lond. A **115**, 700 (1927).

[15] M.Y. Li, *An introduction of mathematical modeling of infectious diseases*, Springer (2018).

[16] D. Stauffer and A. Aharony, *An Introduction to Percolation Theory*, Taylor and Francis (2003).

[17] J. M. Hammersley, D.J.A. Welsh, “First-passage percolation, subadditive processes, stochastic networks and generalized renewal theory”, in *Bernoulli, Bayes, Laplace anniversary volume*, J. Neyman, L.M. LeCam eds., Springer-Verlag (1965), p. 61.

[18] C.D. Howard, “Models of first passage percolation”, in *Probability on discrete structures*, H. Kesten ed., Springer (2004), p. 125–173.

[19] A. Auffinger, M. Damron, J. Hanson, *50 years of FPP*, University Lecture Series 68, American Mathematical Society (2017).

[20] P. Córdoba-Torres, S.N. Santalla, R. Cuerno, J. Rodríguez-Laguna, *Kardar-Parisi-Zhang universality in first passage percolation: the role of geodesic degeneracy*, J. Stat. Mech. 063212 (2018).

[21] D.B. Abraham, L. Fontes, C.W. Newman, M.S.T. Piza, Phys. Rev. E **52**, R1257 (1995).

[22] S. Beyme, C. Leung, Ad Hoc Netw. **17**, 60 (2014).

[23] G. Kordzakhia, S.P. Lalley, Stoch. Proc. App. **115**, 781 (2005).

[24] R. Bündschuh, T. Hwa, Discr. Appl. Math. **104**, 113 (2000).

[25] L.M. Sander, C.P. Warren and I.M. Sokolov, *Epidemics, disorder, and percolation*, Physica A, **325**, 1, (2003).

[26] J.C. Miller, *Percolation and epidemics in random clustered networks*, Phys. Rev. E **80**, 020901(R) (2009).

[27] G. Oliveira, *Early epidemic spread, percolation and Covid-19*, Journal of Mathematical Biology **81**, 1143 (2020).

[28] F. Croccolo and E. Romanba, *Spreading of infections on random graphs: A percolation-type model for COVID-19*,

Chaos, Solitons & Fractals, **139**, 110077, (2020).

[29] D. Villarrubia, I. Álvarez Domenech, S.N. Santalla, J. Rodríguez-Laguna, P. Córdoba-Torres, *First-passage percolation under extreme disorder: from bond-percolation to KPZ universality*, Phys. Rev. E **101**, 062124 (2020).

[30] L. C. Freeman *Centrality in social networks conceptual clarification*. Social Networks **1**, 215 (1979).

[31] T.H. Cormen, C.E. Leiserson, R.L. Rivest, C. Stein, *Introduction to algorithms*, The MIT Press (1990).

[32] C.M. Schneider, T. Mihaljev, S. Havlin and H.J. Herrmann, *Suppressing epidemics with a limited amount of immunization units*, Phys. Rev. E **84**, 061911 (2011).

[33] O. Toledano, B. Mula, S. N. Santalla, O. Gálvez, J. Rodríguez-Laguna, 2021, Epidemic Modelling UNED website, <https://sites.google.com/view/epidemic-modelling-uned/home>.